A&A 489, 395–402 (2008)
DOI: 10.1051/0004-6361:200810147

Astronomy & Astrophysics

Production of ^{26}Al by super-AGB stars

L. Siess and M. Arnould

Institut d'Astronomie et d'Astrophysique, Université Libre de Bruxelles, CP 226, 1050 Brussels, Belgium
e-mail: siess@astro.ulb.ac.be

Received 7 May 2008 / Accepted 17 July 2008

ABSTRACT

Context. Super AGB (SAGB) stars have initial masses ranging between ~7–11 $M_\odot$ and develop efficient hydrogen burning at the base of their convective envelope during their AGB evolution, leading to a substantial production of $^{26}Al_g$.

Aims. We present the first discussion of the contribution of the SAGB stars to the galactic $^{26}Al_g$ production, and we estimate the main uncertainties that affect the determination of the $^{26}Al_g$ yields.

Methods. The results of full stellar evolution computations are presented, with special emphasis on the $^{26}Al_g$ yields from SAGB stars. We also use a postprocessing nucleosynthesis code to quantify the uncertainties associated with the nuclear reaction rates and with the treatment of convection that modifies the thermodynamical conditions at the base of the convective envelope.

Results. Hot bottom burning leads to individual SAGB $^{26}Al_g$ yields that are larger than those from intermediate mass stars, amounting to typical values as high as 5×10^{-5} $M_\odot$. The overall SAGB contribution remains modest, however, not exceeding ~0.3 $M_\odot$ of the estimated galactic content of 2.8 $M_\odot$. On the other hand, the SAGB $^{26}Al/^{27}Al$ ratios always exceed 0.01, which is commensurable with the values measured in some SiC grains considered to originate in C-rich AGB stars. However, the isotopic composition of some other elements, particularly nitrogen, is clearly at variance with the observations. We find that the $^{26}Al_g$ yields are not affected by the pollution induced by the third dredge-ups, but that they strongly depend on the evolution of the temperature at the base of the convective envelope, the determination of which remains highly dependent on the specific convection model used in the stellar computations. Modifications of T_{env} by ±10% leads to variations in the $^{26}Al_g$ yields by a factor of 0.2 to 6. In comparison, the nuclear reaction rate uncertainties have less of an impact, altering the yields by less than a factor of 2.

Key words. nuclear reactions, nucleosynthesis, abundances – stars: AGB and post-AGB – stars: evolution – gamma rays: observations

1. Introduction

The radionuclide ^{26}Al (half-life $t_{1/2} = 7.4 \times 10^5$ yr) is of substantial interest in cosmochemistry and in γ-ray line astrophysics. Its presence in a 'live' form during the early stages of the solar system is demonstrated by the observed excesses of its daughter isobar ^{26}Mg correlated with the ^{27}Al content for a variety of meteoritic materials. The $^{26}Al/^{27}Al$ ratio at the time of trapping into solar system solids (especially CAI calcium-aluminum-rich inclusions) is now estimated to be typically 6–7 $\times$ 10^{-5} (e.g. Wadhwa et al. 2007 for references). Larger ratios ranging all the way between sometimes 10^{-4} to values in excess of 0.1 are also inferred to have been present in certain presolar grains of stardust (silicon carbides, silicon nitride, graphite, oxides).

Likely injectors of ^{26}Al in the solar nebula are very massive stars evolving through a Wolf-Rayet phase to Type Ib/c supernovae. The Wolf-Rayet winds during the WC-WO phase are loaded with ^{26}Al and with some of the other short-lived radionuclides (Palacios et al. 2005; Arnould et al. 2006) inferred to have been present in the primitive solar nebula along with ^{26}Al (as listed by e.g. Meyer & Zinner 2006). Important enough, a complement of radionuclides, including ^{60}Fe, are produced just before being ejected by the explosion at the Type Ib/c supernova stage (Limongi & Chieffi 2006). Less massive stars ending their evolution as Type II supernovae are also potential injectors. Their ^{26}Al and ^{60}Fe yields are discussed by Limongi & Chieffi (2006). The plausibility that (very) massive stars have been efficient contaminators is discussed in qualitative terms by Arnould et al. (1997), and a more specific scenario is proposed by Ouellette et al. (2007). The plausibility of other proposed stellar sources such as asymptotic giant branch stars (Mowlavi & Meynet 2000) or novae (e.g. José et al. 1997) is generally considered to be weak. They can just produce a fairly limited variety of relevant radionuclides[1].

The higher concentration of ^{26}Al than of ^{27}Al in some stardust grains (see above) may also originate from supernovae. However, carbon-rich AGB stars of different metallicities seem to be the main source. The production of ^{26}Al in AGB stars with metallicities in the $0.008 \leq Z \leq 0.02$ range and with masses ranging from 1.75 to 5 $M_\odot$ has been re-examined recently by van Raai et al. (2008) with special emphasis on the uncertainties of nuclear origin. Their predictions can be made compatible with the grain data under some restrictive conditions regarding the nuclear reaction rates.

On top of its major cosmochemical interest, ^{26}Al has also played a key role in the development of γ-ray line astrophysics with the observation of the 1.8 MeV γ-ray line resulting from the de-excitation of the first excited state of ^{26}Mg populated by the ^{26}Al β-decay (Prantzos & Diehl 1996, for a review; see also Diehl 2006). The RHESSI and INTEGRAL satellites are providing improved quality data with respect to the COMPTEL

[1] Instead of "external" radionuclide sources, such as massive stars, an in situ production has also been envisioned. It originates from the irradiation of the solar nebula by energetic particles accelerated by the young Sun. This process is required to account for the presence of ^{10}Be ($t_{1/2} = 1.5 \times 10^6$ yr) and of the very short-lived ^{7}Be ($t_{1/2} = 53$ days) in the early solar nebula. Some other radionuclides of relevance can be synthesised concomitantly (Gounelle et al. 2006).

measurements. The derived 1.8 MeV map clearly points to an emission located in the inner Galactic radian and from the Cygnus region (Knödlseder et al. 2008), and a total steady mass of about 2.8 $M_\odot$ is predicted. Another important γ-ray line radionuclide is ^{60}Fe. It seems reasonable to assume that it has a galactic distribution similar to the ^{26}Al one. If so, a value of 0.148 ± 0.06 is derived for the ^{60}Fe/^{26}Al ratio of γ-ray fluxes. A massive star origin for ^{26}Al has been convincingly demonstrated by Knödlseder (1999) on the grounds of the galactic distribution of its γ-ray flux. In fact, the main ^{26}Al and ^{60}Fe data are compatible with the production of ^{26}Al and of ^{60}Fe by massive stars evolving to Type Ib/c or Type II supernovae. However, the uncertainties of various origins affect the predictions (Limongi & Chieffi 2006), so that it is difficult at this point to ascertain the relative importance of the steady winds from WC-WO stars and of the Type Ib/c and Type II supernovae explosions in the total ^{26}Al budget of the interstellar medium (Knödlseder 2008).

Among the questions that remain unanswered is the possible contribution to this budget from the super-AGB (SAGB) stars in the approximate 7 to 11 $M_\odot$ range. No calculation of the ^{26}Al production by these stars has ever been conducted, and the cosmochemistry or γ-ray-line astrophysics literature sweep the SAGB stars totally under the rug, or at best assumes that they do not produce ^{26}Al (e.g. Limongi & Chieffi 2006). The aim of this paper is to report on the first calculations of the SAGB yields of this radionuclide, and to compare them with the predicted values for the immediately neighbouring lower and higher mass stars.

2. The super-AGB models

We computed the evolution of non-rotating SAGB stars with various masses and metallicities in the overall ranges $7.5 \leq M \leq 10.5\ M_\odot$, and $0.0001 \leq Z \leq 0.04$. Table 1 summarizes some properties of these models and includes the initial helium content (Y), the ^{26}Al$_g$ yields (M_{26}), the He core ($M_c^{\rm TP}$) and total stellar mass ($M^{\rm TP}$) at the first thermal pulse, the maximum temperature reached at the base of the convective envelope ($T_{\rm env}^{\rm max}$), an estimate of the average envelope temperature as defined by $\overline{T_{\rm env}} = \int T_{\rm env}\,{\rm d}t / \int {\rm d}t$, where the integration starts from the time of occurrence of the 2DUP, and the time $\Delta t_{\rm env}$ during which $T_{\rm env} > \overline{T_{\rm env}}$.

2.1. Input physics

Our SAGB models were computed with the same version of STAREVOL as described in Siess (2006, 2007a, hereafter Paper I). For the needs of our study, we recall that the mass-loss rate follows the Vassiliadis & Wood (1993) prescription and that no metallicity dependence is taken into account. The rates for the key nuclear reactions involved in the NeNa and MgAl chains are the adopted rates from the NACRE compilation (Angulo et al. 1999) except for the ^{26}Al$_g$(p,γ) rate that is adopted from Iliadis et al. (2001). Our network includes 53 species (n, ^{1,2}H, ^{3,4}He, ^{6,7}Li, ^{8,10,11}B, ^{7,9}Be, ^{12,13,14}C, ^{13,14,15}N, ^{15,16,17,18}O, ^{18,19,20}F, ^{20,21,22,23}Ne, ^{22,23,24,25}Na, ^{24,25,26,27}Mg, ^{26g,26m,27}Al, ^{28,29,30}Si, ^{31}P, ^{32,33,34,35,36}S, ^{35,36,37}Cl, plus a fake element called Heavy that accounts for all the other species) and 177 nuclear reactions that take all major nuclear (n-, p-, α-captures), weak (electron captures, β-decays) and electromagnetic (photodisintegration) interactions into account. The ^{13}N(p,γ) and ^{18}F(p,α) reactions of the hot CNO cycles are included and the 2 isomeric states of ^{26}Al are considered as 2 distinct species.

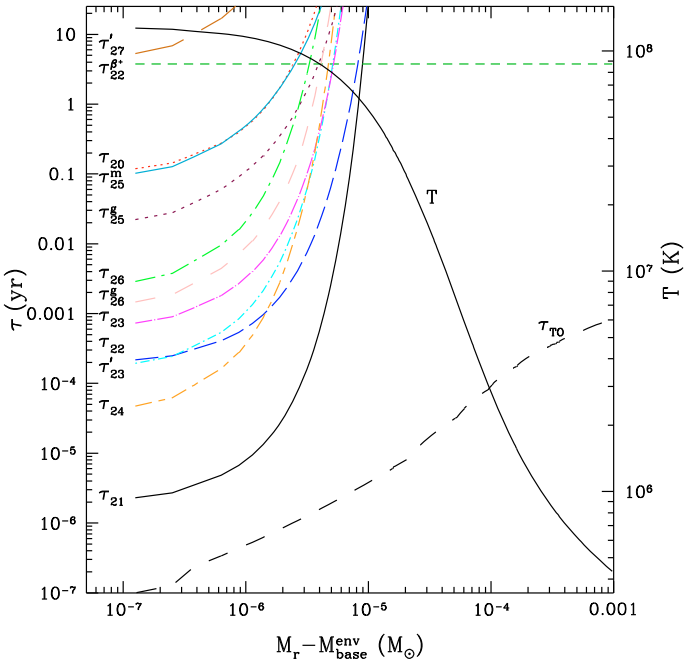

Fig. 1. Mixing ($\tau_{\rm TO}$) and nuclear (τ_i) timescales associated with the nucleosynthesis of ^{26}Al$_g$ as a function of the mass coordinate inside the envelope of a representative 8.5 $M_\odot$, $Z = 0.001$ SAGB model (star II) during the interpulse period. The temperature profile is also shown in thick solid line, right abscissa. The mass coordinate and temperature at the base of the envelope are $M^{\rm env}_{\rm base} = 1.2017\ M_\odot$ and $T_{\rm env} = 1.3 \times 10^8$ K, respectively. The long-dashed line represents the timescale for mixing by convection from $M^{\rm env}_{\rm base}$ to the mass coordinate M_r. The timescale τ_i is associated with the lifetime of the stable nuclide ^{i}X against radiative proton capture; τ'_{23} corresponds to ^{23}Na(p,α) and τ'_{27} to ^{27}Al(p,α); τ^m_{25} and τ^g_{25} relate to the production of ^{26}Al$_{\rm m}$ and ^{26}Al$_{\rm g}$, respectively; τ^g_{26} refers to the reaction ^{26}Al$_g$(p,γ); $\tau^{\beta+}_{22}$ is the β-decay lifetime of ^{22}Na.

The screening factors are taken into account following the formulation given by Mitler (1977). In the convective zones, the nucleosynthesis is computed in one-zone approximation with mass-averaged reaction rates. This assumption is valid as long as the timescale for the reactions of interest remains longer than the convective turnover timescale. To justify this approximation and provide better insight into the internal structure of a typical SAGB, we have plotted in Fig. 1 the temperature profile, as well as several characteristic timescales as a function of the mass coordinate throughout the convective envelope. The turnover timescale $\tau_{\rm TO}$ depicted in this figure is defined as the mixing timescale between the base of the envelope (located at shell $k = 0$, mass coordinate $M^{\rm env}_{\rm base}$) and any given point inside the envelope (shell k, mass coordinate M_r). It is given by

$$\tau_{\rm TO}[k] = \sum_{j=1}^{k} [(r_{j+1} - r_j)^2 / D_{j+1/2}],$$

where the diffusion coefficient comes from the mixing length theory ($D = v_{\rm conv} \times \alpha_{\rm MLT} H_P/3$, with $v_{\rm conv}$ and H_P denoting the convective velocity and pressure scale height, respectively). The first important point to emphasise is that nucleosynthesis only operates in a tiny fraction of the envelope mass ($\lesssim 10^{-4}\ M_\odot$). Second, the mixing timescale between the base of the envelope and the top of the burning region (T of a few 10^6 K) is very short, of the order of a few days ($\tau_{\rm TO} \simeq 10^{-4}$ yr). This mixing timescale remains much shorter than all the relevant nuclear timescales involved in the nucleosynthesis, thus allowing an efficient mixing

of the considered species with the abundant supply coming from the unburnt envelope material. The time needed for a convective globule to reach the surface is, however, much longer because of the decreasing efficiency of convection in the cooler and extended outer regions of the envelope where $T \lesssim 10^5$ K. The envelope turnover timescale decreases along the AGB, from a few tens of years after the 2DUP down to a few years near the tip of the SAGB. For the sake of completeness and to quantify the effects of our one-zone approximation, we also implemented the possibility in our postprocessing code of simultaneously solving the full system of equations coupling mixing and nucleosynthesis (see Sect. 3.1). The results of our simulations confirm that the one-zone approximation remains a valid (and fast) approach to modelling the nucleosynthesis in SAGB stars experiencing efficient HBB. Finally, no extra mixing has been included, and the Schwarzschild criterion has been used to delineate the convective boundaries. The initial composition is scaled solar according to the Grevesse et al. (1996) mixture (for details, see Paper I and Table 1).

2.2. Selected evolutionary properties of thermally pulsing SAGB stars

It is not the aim of this paper to describe the properties of thermally pulsing SAGB stars at length (this analysis is postponed to a forthcoming paper; Siess 2008, in preparation), but rather to concentrate on specific quantities that have a significant impact on the synthesis and yields of ^{26}Al$_g$. In this context, we focus our discussion on the temperature at the base of the convective envelope that controls the ^{26}Al$_g$ surface abundance.

After the completion of the second dredge-up (2DUP) and the termination of carbon burning, energy is mainly provided by a thick He-burning shell (HeBS). The oxygen-neon core deprived of an energy supply starts contracting and radiates aways its internal energy via neutrino emission. The cooling core becomes more degenerate and, as the result of contraction, the HeBS gets thinner and approaches the H-burning shell (HBS). The nuclear energy production is progressively transferred from the active HeBS to the HBS until the latter takes over the entire nuclear energy production.

During this so-called *early-AGB* (e-AGB) phase that ends with the development of the first He-shell flash, the temperature at the base of the convective envelope ($T_{\rm env}$) continuously increases from a few 10^7 K at the end of the 2DUP up to $\sim 1.4 \times 10^8$ K when the first pulse occurs (Fig. 2). These conditions are favourable to nuclear processing at the base of the envelope referred to as hot bottom burning (HBB). During the subsequent thermally pulsing super-AGB (TP-SAGB) phase, the evolution is very similar to that of intermediate-mass AGB stars with alternate H and He-burning modes and the development of recurrent instabilities in the HeBS. However, some noticeable differences are also predicted. Owing to their higher core mass (the minimum mass of a degenerate oxygen-neon core was estimated in Paper I to be $\gtrsim$1.05 $M_\odot$), the gravitational pull is stronger and the layers surrounding the degenerate core more compressed. The HBS and HeBS are thinner and their temperature also higher, exceeding 3.2×10^8 K at the base of the pulse in all our models, thus allowing for the activation of the ^{22}Ne(α,n) neutron source. The mass of the convective He-shell instability is only a few 10^{-4} $M_\odot$, compared to 10^{-2} $M_\odot$ in a corresponding 5 $M_\odot$ AGB star. Because the radiative pressure is not negligible in the HeBS (it contributes to more than 10% of the total pressure), the thermal pulses are shorter lived (a few years at most) and weaker ($L_{\rm He} \lesssim 10^6$ $L_\odot$),

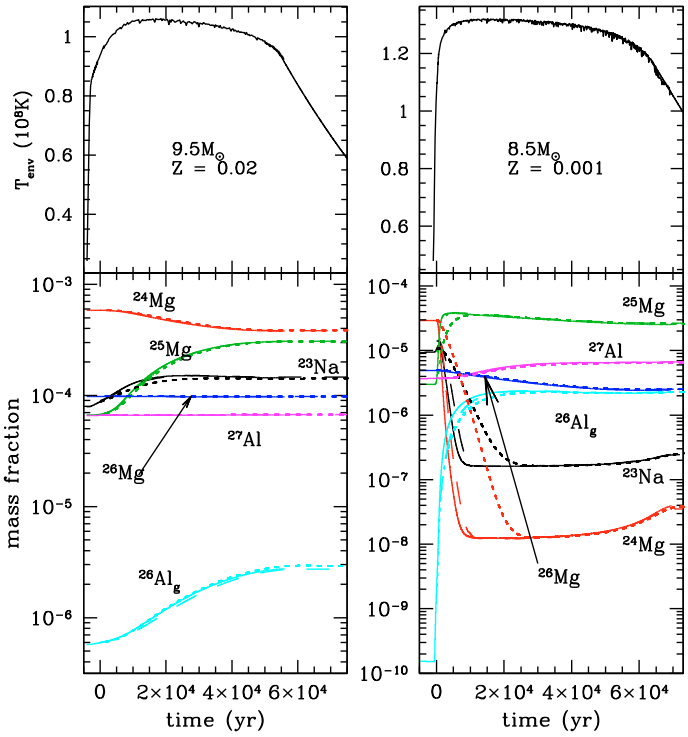

Fig. 2. Evolution of the temperature at the base of the convective envelope (*upper panels*) and of selected surface mass fractions of the nuclides entering the nucleosynthesis of ^{26}Al$_g$ (*lower panels*) for the $M = 9.5$ $M_\odot$ with $Z = 0.02$ star (referred to as star I) and for the $M = 8.5$ $M_\odot$ and $Z = 0.001$ star (referred to as star II). The origin of time coincides with the beginning of the e-AGB phase. The solid lines represent the abundances computed with STAREVOL, the (almost perfectly super-imposed) dashed lines to the synthetic model in the one-zone approximation (Sect. 3.1) and the dotted lines to the solution where mixing and burning are coupled.

and the interpulse periods are reduced to a few hundred/thousand years. Noticeable enough, our adopted treatment of convection does not allow the development of third dredge-up (3DUP) episodes. These are more difficult to trigger because of the weakness of the pulses that result from the more massive core.

As mass is removed from the envelope by strong winds[2], the temperature at the base of the convective zone declines after reaching a maximum value at the beginning of the TP-SAGB phase (Fig. 2). The change in $T_{\rm env}$ affects both the surface luminosity and nucleosynthesis, with an eventual quenching of the HBB. The mass-loss rate also decreases near the end of the evolution.

The evolution of the surface composition is governed by HBB (the possible effect of 3DUPs, if they would indeed develop, is discussed in Sect. 3.3). It is illustrated in Fig. 2 for two representative stars characterised by a value of $T_{\rm env}$ that is moderately high (star I : 9.5 $M_\odot$, $Z = 0.02$) or very high (star II : 8.5 $M_\odot$, $Z = 0.001$). To understand the different abundance trends, we base our analysis on the discussion of nuclear timescales as shown for some relevant reactions in the lower panel of Fig. 3. It must be kept in mind, however, that these nuclear timescales are mass-averaged timescales and that the temperature indicated in Fig. 3 does not correspond to the temperature at which they were estimated. They should thus be considered as *effective* envelope nuclear timescales. The

[2] With our prescription, mass-loss rates as high as 10^{-4} $M_\odot$ yr^{-1} can be reached.

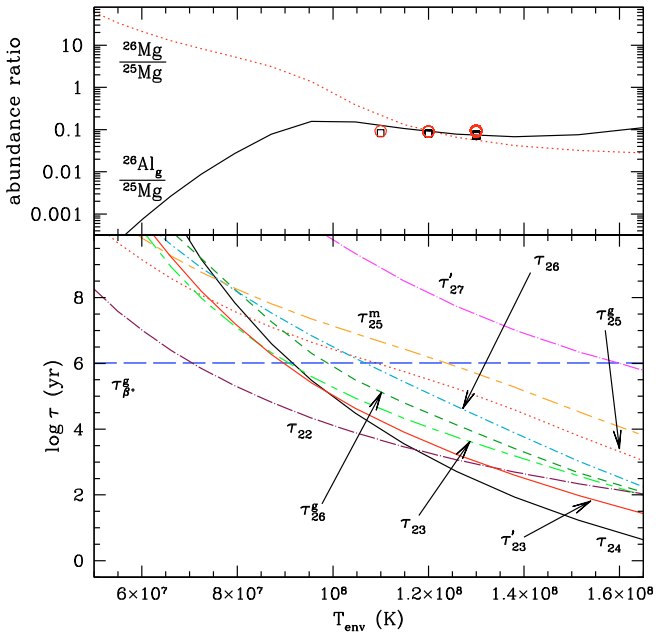

Fig. 3. *Lower panel:* nuclear timescales in our one zone model approximation of the main reactions involved in the MgAl chain as a function of the temperature $T_{\rm env}$ at the base of a typical SAGB envelope. We use the same notation for τ_i as in Fig. 1 except that in this plot the timescales are estimated from a mass-averaged cross section. $\tau^g_{\beta^+}$ is the β-decay lifetime of ^{26}Al$_{\rm g}$. *Upper panel:* equilibrium abundance ratios of ^{26}Al$_{\rm g}$/^{25}Mg (solid line) and ^{26}Mg/^{25}Mg (dotted line) as a function of $T_{\rm env}$. Open squares and circles represent the ^{26}Al$_{\rm g}$/^{25}Mg and ^{26}Mg/^{25}Mg ratios coming from the full models of star II at selected temperatures. Star I never develops temperatures high enough for equilibrium to be reached.

evolution of the ^{23}Na abundance is dictated by a competition between its production by proton captures on ^{22}Ne and its destruction through (p,α) and (p,γ) reactions. For $T_{\rm env}$ below about 9×10^7 K, the (p,α) channel is quicker than the (p,γ) one, so that an NeNa cycle can develop, leading to equilibrium abundances of the involved nuclides. This situation is barely reached in star I ($T_{\rm env} \sim 10^8$ K), and translates into a ^{23}Na equilibrium abundance that is greater than its initial value. In addition, for star I the lifetime τ_{23} of ^{23}Na against (p,γ) captures[3] is roughly comparable to the duration of the SAGB phase ($\tau_{\rm SAGB} < 10^5$ yr), so that only a slight amount of ^{23}Na is burnt into ^{24}Mg at the end of the computed evolution. The situation is different in star II, where $T_{\rm env} \sim 1.3\times10^8$ K. At these temperatures, ^{23}Na is more rapidly transformed into ^{24}Mg than destroyed by (p,α), so that no equilibrium NeNa cycle can be established. In addition, $\tau_{23} \ll \tau_{\rm SAGB}$, which leads ^{23}Na to be depleted early in the AGB evolution. Note, however, that, compared to the NACRE "adopted" rates, the Iliadis et al. (2001) "recommended" values lead to faster (p,γ) reactions and, below $T < 40\times10^6$ K, to slower (p,α) reactions. Adopting these newer rates increases the leakage to the MgAl chain and consequently affects the final ^{23}Na and ^{24}Mg abundances (see also Sect. 3.2). It has to be acknowledged that the situation is by far less clear-cut when the rate uncertainties reported in the two compilations, which are still quite large in the temperature range of interest here, are duly taken into account. (The limits on the rates reported by Iliadis et al. are well within the range of uncertainties reported by NACRE.) As far as ^{24}Mg is concerned, $\tau_{24} \gg \tau_{\rm SAGB}$ in star I, so that its destruction is not efficient. This contrasts with the situation in star II, where ^{24}Mg is even more rapidly destroyed than ^{23}Na, as $\tau_{24} < \tau_{23}$ at $T_{\rm env} \sim 1.3\times10^8$ K. No replenishment of ^{24}Mg is possible from ^{27}Al, because τ'_{27} is much longer than $\tau_{\rm SAGB}$ for both stars. The ^{24}Mg destruction is accompanied by an increase in the ^{25}Mg abundance, which roughly reaches the initial ^{24}Mg content in star II in view of the fact that $\tau^{\rm g}_{25} \sim \tau_{\rm SAGB}$ for the given $T_{\rm env}$ value. In star I, only a small fraction of ^{25}Mg is transformed into ^{26}Al because $\tau^{\rm g}_{25}$ largely exceeds $\tau_{\rm SAGB}$ and the resulting ^{26}Al/^{25}Mg is quite small ($\lesssim10^{-2}$) in this model. The production of ^{26}Al is substantially more in star II as $\tau^{\rm g}_{25}$ becomes comparable to $\tau_{\rm SAGB}$. However, some of the produced ^{26}Al has time to transform into ^{27}Al in star II, which explains the slight ^{27}Al enhancement with time. This is not possible in star I. The ^{26}Al^g β^+-decay is always too slow to affect the ^{26}Al abundance.

As protons have time to be captured by both ^{25}Mg and ^{26}Al during the star II SAGB phase, it is expected that the ^{26}Al/^{25}Mg ratio can reach an equilibrium value equal to the ratio of the proton capture rates by ^{25}Mg and by ^{26}Al. This is not the case in star I with a lower $T_{\rm env}$ value. These expectations are confirmed by the detailed abundance computations, as shown in Fig. 3. From this, one may conclude that the ^{26}Al/^{25}Mg ratio is independent of metallicity *at a given temperature*, provided it is high enough. With decreasing metallicity, the base of the envelope is hotter ($T_{\rm env} \gtrsim 1.4\times10^8$ K) and ^{26}Al$_{\rm g}$ is more efficiently depleted, but the equilibrium ratios remain almost constant.

3. The Super-AGB ^{26}Al yields

3.1. Postprocessing nucleosynthesis code

We have developed a simple nucleosynthesis code that reprocesses the data given by the full computations. This code allows a safe investigation of the effects of changing the still uncertain rate of ^{26}Al$_{\rm g}$(p,γ), since this reaction does not contribute to the overall nuclear energy production significantly. It also permits the impact of the 3DUP to be examined if it were to develop in the considered stars. In view of remaining uncertainties in the treatment of convection, the existence of a 3DUP cannot be ruled out in spite of its absence in our detailed model calculations. Even then, its efficiency would be hard to predict.

The procedure adopted in the postprocessing code is as follows. The initial composition is taken from the stellar models at the beginning of the e-AGB phase, before $T_{\rm env}$ increases substantially, and after the 2DUP is completed. The evolution of the surface luminosity (L), radius (R), and $T_{\rm env}$ are then approximated by fitted curves as a function of the envelope mass and time. We use a "representative" envelope structure[4] and, at each time, the temperature and mass profiles are scaled to coincide with the current values of $T_{\rm env}$ and M. The HBB nucleosynthesis in the envelope is computed in a one-zone model approximation with a mass-averaged reaction rate, as in the stellar evolution code. At the next timestep, the new values of L, R, and $T_{\rm env}$ are estimated from the fits. The mass-loss rate is recomputed (using L and R and the number compared to the full stellar models), the envelope structure is updated to take the change in $T_{\rm env}$ and

[3] Here and in the following, τ_i refers to the lifetime of the stable nuclide i against radiative proton capture; see also Fig. 3. If otherwise specified, this nuclear timescale is estimated in the one-zone approximation.

[4] As confirmed by our tests, the results are weakly dependent on the specific choice of the stellar envelope structure, provided the star has fully settled in its TP-SAGB phase.

in mass into account, and the nucleosynthesis is recalculated. The core growth rate ($\dot{M}_{\rm core}$) does not vary much along the TP-SAGB evolution, and an average value is taken from the models. The values are equal to 6×10^{-7} and 6.5×10^{-7} $M_\odot$ yr^{-1} for stars I and II, respectively. The procedure is repeated until the envelope is removed. To model the effect of the 3DUP, part of the intershell composition is mixed into the envelope after each thermal pulse, the mass of which is given by our full models. We use a fixed intershell composition taken from a typical SAGB model after the quenching of the instability. The efficiency of the 3DUP is controlled by the so-called dredge-up parameter $\lambda = \Delta M_{\rm DUP}/\Delta M_{\rm c}$, which is the ratio between the mass dredged-up by the convective envelope ($\Delta M_{\rm DUP}$) and the amount of mass through which the H-burning shell has moved during the previous interpulse phase ($\Delta M_{\rm c}$). In this approach, the envelope is repeatedly polluted by the 3DUPs and subsequently nuclearly processed by HBB during the interpulse phase, which is short in these stars, of the order of 280 and 130 yr in stars I and II, respectively. This model implicitly assumes that the occurrence of the 3DUP does not significantly affect the interpulse evolution of $T_{\rm env}$. This is certainly a good approximation at solar metallicity where the dredge up of C does not greatly affect the physical evolution of the star. As the metallicity decreases, the amount of C dredged up may become comparable and greater than the initial CNO abundance, hence affect the evolution of the H shell and, in turn, that of the He shell. Despite its simplicity, this model accurately reproduces the main evolution of the surface abundances as shown in Fig. 2. It is thus well-suited to quantifing the effects of the uncertainties in some non-energetically relevant nuclear reaction rates, and it allows the effect of the 3DUP on the ^{26}Al yields to be investigated.

To quantify the uncertainties associated in our one-zone approximation, our postprocessing code was upgraded in order to compute the full coupling of the nucleosynthesis and diffusion equations. In this scheme, the evolution of a given species i (molar mass fraction Y_i) is given by

$$\frac{{\rm D}Y_i}{{\rm D}t} = \frac{\partial}{\partial m}\left[\left(\frac{\partial m}{\partial r}\right)^2 D \frac{\partial Y_i}{\partial m}\right] + \text{nuclear terms}$$

where D is the convective diffusion coefficient as defined in Sect. 2.1. The results are shown in Fig. 2. As far as the abundance of ^{26}Al$_{\rm g}$ is concerned, the differences between the two treatments are negligible. These approaches reveal however, some discrepancies that mainly affect the nucleosynthesis of ^{23}Na and ^{24}Mg when the temperature at the base of the envelope is very high (star II). Although the final mass fraction converges to the same value, ^{23}Na and ^{24}Mg are depleted more rapidly in the one-zone approximation. The main reason for this behavior comes from the fact that in the inner part of the envelope (where $T \gtrsim 80 \times 10^8$ K) the rate of ^{23}Na(p,γ) overcomes that of ^{23}Na(p,α), while the opposite is true in the more external and cooler layers where $\tau_{23} < \tau'_{23}$ (Fig. 1). In the one-zone model, only one ^{23}Na destruction channel is at work, and this limitation is responsible for the observed differences.

This tools is also used to estimate the evolution of the surface abundances during the last thermal pulses. Indeed, owing to convergence problems near the end of the TP-SAGB phase, the computations were stopped. During the remaining evolution, the values of L, R, and $T_{\rm env}$ were extrapolated as a function of the envelope mass.

3.2. Nuclear uncertainties

Recently, van Raai et al. (2008) have investigated the impact of nuclear uncertainties on the ^{26}Al yields from AGB stars. They show that the main uncertainty comes from the ^{26}Al$_{\rm g}$(p,γ) rate, which is especially poorly known at the lowest temperatures for which ^{26}Al has time to capture protons. The uncertainty reduces to a factor of about 10 or less for $T \geq 10^8$ K. The reaction rate data and uncertainties have been kindly provided to us prior to publication by C. Iliadis and implemented in our synthetic model. Figure 4 shows that, between the lower and upper limits of the ^{26}Al$_{\rm g}$(p,γ) rate, the ^{26}Al$_{\rm g}$ abundances vary by a factor of 2 with respect to the standard rate for our hottest star (star II) and by $\pm$10% for star I. This conclusion apparently contradicts the fact that the rate uncertainties increase with deceasing temperatures. It is explained by the reaction rates being averaged over the convective envelope, and thus depending on the temperature and density profiles. At the base of the envelope, the temperature and density are higher in the low-metallicity star II than in star I. As a consequence of these structural differences, the region where the ^{26}Al$_{\rm g}$ is efficiently produced (i.e. where $5 \times 10^7 \lesssim T \lesssim T_{\rm env}$) encompasses a larger mass in star II than in star I. The effects of the nuclear uncertainties on the ^{26}Al$_{\rm g}$ synthesis are thus greater in the former than in the latter star.

To further investigate the effects of nuclear uncertainties, we ran additional simulations with our postprocessing code where the NACRE "adopted" reactions rates for the NeNa and MgAl chains replaced by the Iliadis et al. (2001) "recommended" values. The results are shown in Fig. 4. As pointed out in Sect. 2.2, the Iliadis et al. (2001) compilation provides a faster ^{23}Na(p,γ) rate that enhances the leakage out of the NeNa cycling. This higher rate compared to the NACRE value is responsible for the faster ^{23}Na depletion, and the effect is more pronounced at lower temperatures, in particular in star I. Except for ^{23}Na and potentially ^{24}Mg, the use of the Iliadis rates does not significantly affect the abundances of the other elements. We report a change of $\lesssim\pm$20% in the final ^{26}Al$_{\rm g}$ yields using these two different rate sets. Remaining uncertainties reported by NACRE and by Iliadis et al. might blur the picture further (see Sect. 2.2).

3.3. Effect of the third dredge-up

The procedure described in Sect. 3.1 has also been used to investigate how the 3DUP, if it were to exist, could modify the surface abundance of key elements including ^{26}Al$_{\rm g}$. Figure 5 shows the results of simulations for stars I and II with $\lambda = 0$ (no 3DUP) and $\lambda = 0.7$. As reported in Siess (2007b) for a 9.5 $M_\odot$ $Z = 0.04$ star, the effect of the 3DUP is weak mainly because of the large envelope dilution factors (up to 10^4 to 10^5) that are involved, and that cannot be compensated for by the large number of 3DUPs that is assumed if $\lambda = 0.7$. Note, however, that the 3DUP pollution of the surface is more significant at lower metallicity because of the stronger chemical contrast between the intershell and envelope composition (Siess 2008, in preparation). A contamination of the envelope by the 3DUP could in fact be noticeable near the end of the computed evolution, when the mass of the envelope is substantially reduced, as shown in Fig. 2. The signature of the 3DUPs would furthermore be largely blurred by the efficient HBB.

The high temperatures at the base of the thermal pulse allow He to burn. This burning, as in all TP-AGB stars, is incomplete and, at the time of the 3DUPs, the intershell is strongly enriched in ^{25,26}Mg produced in the pulse by (α,n) and (α,γ) reactions on ^{22}Ne. In the dredged-up material, typical mass

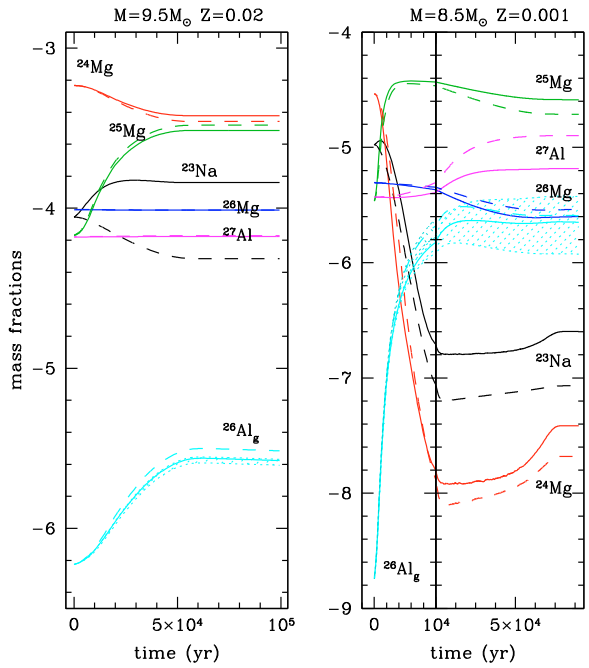

Fig. 4. Effect of nuclear uncertainties on the evolution of the surface abundances of selected nuclides for stars I (*left panel*) and II (*right panel*). The solid and dashed lines refer to the NACRE and Iliadis et al. (2001) rates, respectively. The shaded area shows the possible range of ^{26}Al$_g$ when the nuclear uncertainties on ^{26}Al$_g$(p,γ) rate is accounted for.

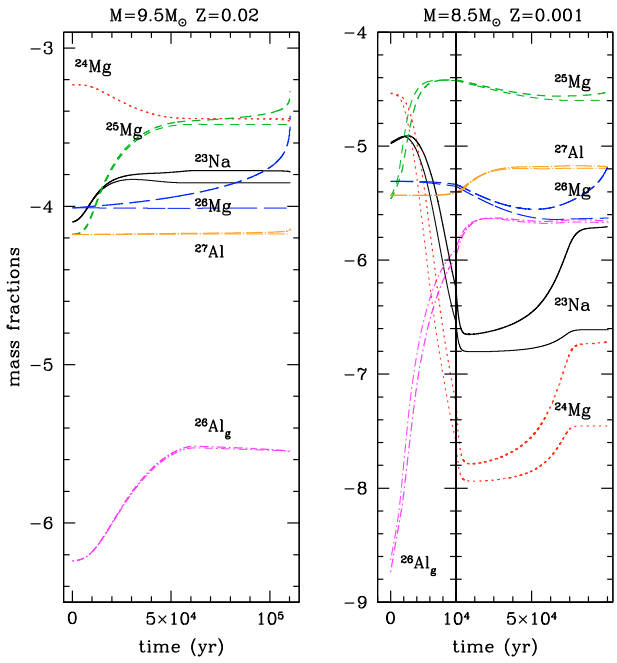

Fig. 5. The impact of 3DUP episodes on the evolution of the surface abundances of selected nuclides for stars I (*left panel*) and II (*right panel*). Simulations with and without envelope pollution by the 3DUPs are represented by thick and thin lines, respectively. The value $\lambda = 0.7$ is assumed when the 3DUP is activated. Typical durations of the interpulse periods are 280 and 130 yr for stars I and II, respectively.

fractions of ^{25}Mg : ^{26}Mg for our representative stars I and II are 1.40×10^{-4} : 1.52×10^{-4} and 3.49×10^{-3} : 4.37×10^{-3}, respectively. Comparison of these numbers with the corresponding surface values indicates (see Fig. 5) that the 3DUP enhances the surface ^{25}Mg and ^{26}Mg abundances by factors ~6–10 and ~50 respectively. In contrast, the ^{26}Al$_g$ amount remains largely insensitive to the presence of the 3DUP. This comes mainly from ^{26}Al$_g$ being efficiently destroyed in the pulses by the captures of neutrons resulting from the ^{22}Ne burning.

3.4. Impact of changing T_{env}

That our predicted surface ^{26}Al$_g$ abundance is rather insensitive to the possible existence of the 3DUP is clearly good news. However, one does not have to overlook that a change in the convection efficiency (through a change in the value of the MLT parameter α or by using a different convection model) could also have a strong influence on the efficiency of the HBB (Sackmann & Boothroyd 1991; Ventura & D'Antona 2005) through changes in $T_{\rm env}$. The surface luminosity would also be affected, along with the mass-loss rate, hence the duration of the SAGB phase and the number of pulses. The bottom line would be a significant alteration of the surface CNO, ^{23}Na, and ^{24}Mg abundances, as shown in Ventura & D'Antona (2005) in their study of a 5 $M_\odot$ model. To assess these effects in SAGB stars, we used our synthetic code and artificially increase and decrease $T_{\rm env}$ by ±10%, which roughly corresponds to the change in magnitude observed by Ventura & D'Antona (2005) in their full stellar models. It should be noted that our adopted mass-loss rate is not affected by the change in $T_{\rm env}$, so these results should only be considered as qualitative rather than quantitative. Figure 6 illustrates that the impact of changing $T_{\rm env}$ is quite significant. For star I, an increase in $T_{\rm env}$ by 10% boosts the ^{26}Al$_g$ production, so that its final abundance is a factor ~6 higher. This is not the case for star II, since the temperature in this model becomes so high that ^{26}Al$_g$ is efficiently destroyed by (p,γ) reactions. When decreasing $T_{\rm env}$, proton captures on ^{25}Mg are reduced and ^{26}Al$_g$ is burnt more slowly, resulting in an overall less efficient ^{26}Al$_g$ production. The different thermodynamical conditions found at the base of the convective envelope lead to large variations in the yields. For star I, the ^{26}Al$_g$ yield varies by a factor of 0.4 to 6 compared to its nominal value; for star II, it is lowered by a factor of 0.3 to 0.7. The problem of precisely determining the convective boundaries thus appears to be the main source of uncertainty affecting the ^{26}Al$_g$ yields.

3.5. Galactic yields

To determine the contribution of massive AGB stars to the galactic ^{26}Al$_g$ production, we proceed as described in Prantzos & Diehl (1996). The AGB stars more massive than $M_1 \sim 3$–$4\ M_\odot$ produce most of their ^{26}Al$_g$ in the last 10^6 yr of their TP-AGB evolution. This is less than the lifetime of this nuclide, so we can reasonably assume that the ejected mass represents what is indeed present in the interstellar medium. Stars with lower masses ($M_1 < 3\ M_\odot$) are not expected to contribute significantly to the yields (e.g. Prantzos & Diehl 1996).

We assume a Salpeter (1955) initial mass function (IMF) $f(m) = AM^\gamma$, where the power law index is $\gamma = -2.35$, and the constant A is given by the normalisation condition

$$\int_{0.1}^{120} f(m)\mathrm{d}m = 1. \quad (1)$$

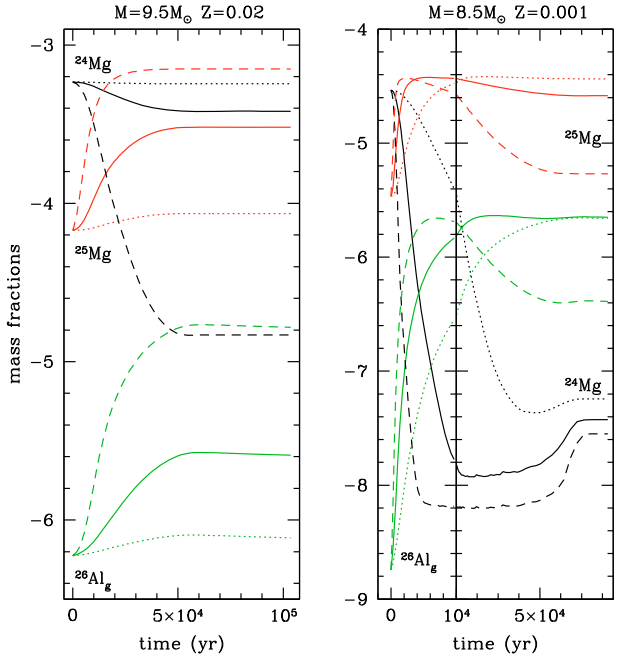

Fig. 6. Effect of changing $T_{\rm env}$ on the evolution of the surface abundances of selected nuclides for stars I (*left panel*) and II (*right panel*). The solid line corresponds to the full stellar models, while the dashed and dotted lines come from the synthetic computations where $T_{\rm env}$ was artificially increased and decreased by a factor of 1.1 and 0.9, respectively.

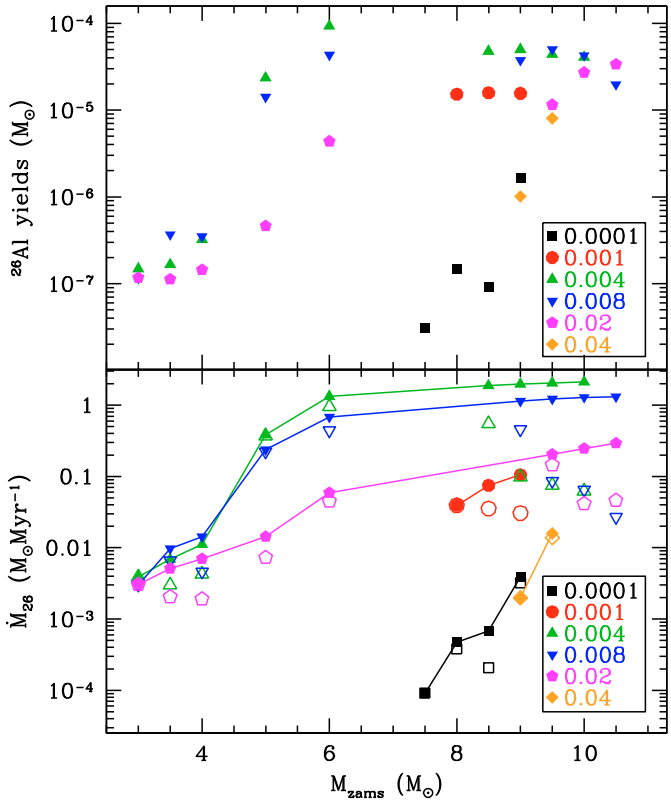

Fig. 7. *Upper panel*: ^{26}Al$_{\rm g}$ yields (in $M_\odot$) as reported in Table 1 for $7.5 \le M_{\rm ZAMS}/M_\odot \le 10.5$, and from the Karakas & Lattanzio (2007) models for $M_{\rm ZAMS} \le 6\ M_\odot$; *lower panel*: open symbols represent the ^{26}Al injection rate (in $M_\odot$ yr^{-1}) as a function of the initial mass for different metallicities. Filled symbols connected by solid lines show the cumulative function defined as $\sum \dot{M}_{26}$.

The average mass of ^{26}Al$_{\rm g}$ ejected by stars in the mass range $[M_1, M_2]$ is

$$\langle m_{26}\rangle = \frac{\int_{M_1}^{M_2} M_{26}(m) f(m) {\rm d}m}{\int_{M_1}^{M_2} f(m) {\rm d}m}, \quad (2)$$

where $M_{26}(m)$ is the mass of ^{26}Al$_{\rm g}$ ejected by the star of mass m, as given by our stellar models (Table 1), $M_1 \sim$ 3–4 $M_\odot$, and M_2 is the upper mass of SAGB stars. Its value is sensitive to metallicity and extra-mixing processes (Siess 2007a), and corresponds approximately to the highest value of $M_{\rm ZAMS}$ provided in Table 1. The ^{26}Al injection rate (in $M_\odot$ yr^{-1}) then writes as

$$\dot{M}_{26} = \langle m_{26}\rangle f_{\rm MAGB}, \quad (3)$$

where $f_{\rm MAGB}$ is the frequency of stars occurring in the mass range $[M_1,M_2]$, and $f_{\rm MAGB}$ is related to the star formation rate (SFR) Ψ by

$$f_{\rm MAGB} = \Psi \frac{\int_{M_1}^{M_2} f(m){\rm d}m}{\int_{0.1}^{120} m f(m){\rm d}m}\cdot \quad (4)$$

In the simple model adopted here, the SFR and IMF are assumed to be universal and constant. The SFR is estimated to range between ~3–5 $M_\odot$ yr^{-1} (e.g. Prantzos & Aubert 1995) which, for our adopted IMF, corresponds to a stellar birthrate $\dot{N} = \Psi / \int_{0.1}^{120} m f(m){\rm d}m \sim 10$ stars yr^{-1}.

Figure 7 shows that, above $Z = 0.001$ where we have data for $M \le 6\ M_\odot$, the ^{26}Al$_{\rm g}$ yields from the SAGB stars are higher than those of intermediate mass AGB stars. However the overall contribution at $Z = 0.02$, expressed as the ejected mass $\dot{M}_{26} \times \tau^g_{\beta^+}$ of ^{26}Al$_{\rm g}$ before any β-decay, never exceeds 0.3 $M_\odot$, which represents only a small fraction of the total galactic ^{26}Al$_{\rm g}$ content of 2.8 $M_\odot$. This conclusion is largely robust to uncertainties in nuclear reaction rates and in uncertainties concerning the efficiency of the 3DUP, and is in line with the prevailing wisdom that more massive stars are the main producers of ^{26}Al. In an extensive study of ^{26}Al$_{\rm g}$ production in low and intermediate AGB stars ($M \le 6\ M_\odot$), Mowlavi & Meynet (2000) obtained a slightly higher value for the ^{26}Al yields of ~0.2 $M_\odot$, with roughly half of it coming from stars with $M \ge 5\ M_\odot$. The larger ^{26}Al$_{\rm g}$ production in the Mowlavi & Meynet models is most certainly a consequence of their use of the Reimers (1975) mass-loss rate, which is lower than the Vassiliadis & Wood (1993) prescription used by Karakas & Lattanzio (2007). Indeed, with a shorter TP-AGB evolution, the rise in $T_{\rm env}$ is halted earlier, and the ^{26}Al$_{\rm g}$ production is consequently reduced. Nevertheless, the yields derived by Mowlavi & Meynet (2000) remain within the uncertainties, in good agreement with our results.

Interestingly, we note that, at the metallicities of the Magellanic clouds, massive AGB stars are in general able to produce relatively large amounts of ^{26}Al$_{\rm g}$ ranging up to 1–2 $M_\odot$. Conversely, at very low Z, ^{26}Al is efficiently depleted because of the very high values of $T_{\rm env}$, so that the overall ^{26}Al$_{\rm g}$ production by SAGB stars is small but it may be compensated for by a contribution coming from their lower mass counterparts.

Table 1. Selected properties of our SAGB models as a function of initial mass ($M_{\rm ini}$) and composition (Z and Y): ^{26}Al$_{\rm g}$ yields M_{26} ($M_\odot$), He core ($M_{\rm c}^{\rm TP}$) and total stellar mass (M^{TP}) at the first thermal pulse ($M_\odot$), the maximum envelope temperature ($T_{\rm env}^{\rm max}$ in unit of 10^8 K), an estimate of the average envelope temperature ($\overline{T_{\rm env}}$ in unit of 10^8 K) and the time $\Delta t_{\rm env}$ (in yr) during which $T_{\rm env} > \overline{T_{\rm env}}$. (See Sect. 2 for definitions.)

$M_{\rm ini}$	Z	Y	M_{26}	$M_{\rm c}^{\rm TP}$	$M^{\rm TP}$	$T_{\rm env}^{\rm max}$	$\overline{T_{\rm env}}$	$\Delta t_{\rm env}$
7.5	10^{-4}	0.248	3.04(–8)	1.085	7.497	1.550	1.425	192377
8.0	10^{-4}	0.248	1.47(–7)	1.144	7.996	1.541	1.441	144410
8.5	10^{-4}	0.248	9.02(–8)	1.197	8.494	1.507	1.439	118976
9.0	10^{-4}	0.248	1.64(–6)	1.255	8.991	1.459	1.420	50356
8.0	0.001	0.249	1.52(–5)	1.130	7.980	1.270	1.191	81025
8.5	0.001	0.249	1.58(–5)	1.196	8.460	1.324	1.241	56527
9.0	0.001	0.249	1.56(–5)	1.251	8.973	1.382	1.340	50821
8.5	0.004	0.253	4.76(–5)	1.124	8.392	1.163	1.070	55998
9.0	0.004	0.253	5.00(–5)	1.203	8.854	1.260	1.195	46918
9.5	0.004	0.253	4.38(–5)	1.256	9.393	1.330	1.290	39233
10	0.004	0.253	4.07(–5)	1.309	9.889	1.438	1.392	18890
9.0	0.008	0.259	3.76(–5)	1.109	8.737	1.105	1.008	56847
9.5	0.008	0.259	5.01(–5)	1.158	8.724	1.166	1.095	45765
10	0.008	0.259	4.26(–5)	1.251	9.786	1.293	1.241	47971
10.5	0.008	0.259	1.97(–5)	1.331	10.298	1.467	1.401	14160
9.5	0.02	0.275	1.16(–5)	1.125	9.081	1.065	0.972	50827
10	0.02	0.275	2.72(–5)	1.190	9.533	1.146	1.073	45752
10.5	0.02	0.275	3.39(–5)	1.254	10.217	1.243	1.186	44927
9.0	0.04	0.302	1.01(–6)	1.037	7.962	0.874	0.801	45864
9.5	0.04	0.302	8.04(–6)	1.110	8.921	0.979	0.874	47729

3.6. The case of ^{26}Al-loaded SiC stardust grains

The ^{26}Al/^{27}Al ratio measured in meteoric SiC stardust grains is generally considered to be amenable to a direct comparison with nucleosynthetic predictions for single stars. These grains are believed to form around AGB stars once they become C-rich in the course of their evolution. The distribution of ^{26}Al/^{27}Al ratios in SiC grains of various subtypes ranges all the way from about 5×10^{-4} to 5×10^{-1} (e.g. Meyer & Zinner 2006, for a review). In our SAGB models, this ratio is always more than 0.01, as in most of the SiC X grains, as well as in a small fraction of SiC A + B grains, and in grains classically presumed to have a nova origin. A fairly large fraction of these ^{26}Al-rich grains are characterised by ^{12}C/^{13}C ratios greater than about 20, which by far exceeds the equilibrium value imposed by HBB in SAGB stars. Some of the SiC grains, however, exhibit values below about 10 that agree much better with the SAGB predictions. Even if the calculated ^{12}C/^{13}C and ^{26}Al/^{27}Al reproduce the data for some SiC grains, the ^{14}N/^{15}N ratios of all the analysed SiC grains never exceed about 10^4, which is lower than the calculated minimum value of about 5×10^4. It is thus likely that none of the presently analysed SiC grains form around massive AGB stars.

4. Conclusions

Massive AGB stars can produce a large amount of ^{26}Al$_{\rm g}$ thanks to the high temperatures at the base of their convective envelope. In fact, although limited to a narrow mass range, SAGB stars produce as much ^{26}Al$_{\rm g}$ as "standard" AGB stars. Still, their present-day overall galactic contribution does not exceed about 0.3 $M_\odot$. This quite modest production is in line with the COMPTEL or INTEGRAL observations that clearly establish a correlation between massive stars and the ^{26}Al$_{\rm g}$ γ-ray emission. On the other hand, the large production of ^{26}Al in SAGB stars leads to high ^{26}Al/^{27}Al ratios that are not compatible with the observations of SiC grains considered to originate in C-rich AGB stars.

We also demonstrate that our conclusions are weakly dependent on the remaining nuclear uncertainties. The ^{26}Al$_{\rm g}$ yields should not strongly depend on the mass-loss rate either, at least if high enough temperatures can be reached at the base of the envelope (as in star II) to ensure the rapid establishment of an equilibrium between the ^{25}Mg and ^{26}Al abundances. In such a situation, the surface ^{26}Al$_{\rm g}$ abundance remains almost constant during the TP-SAGB phase. The poor reliability of the modelling of convection not only has an impact on the estimated mass-loss rates, but it is also identified as the main source of uncertainty in the predicted ^{26}Al$_{\rm g}$ yields from SAGB stars.

Acknowledgements. We are very grateful to C. Iliadis for providing us with his new ^{26}Al$_{\rm g}$(p,γ) measurements prior to publication and to the anonymous referee whose insightful comments helped us clarify the manuscript. L.S. is FNRS Research Associate.

References

Angulo, C., Arnould, M., Rayet, M., et al. 1999, Nucl. Phys. A, 656, 3
Arnould, M., Paulus, G., & Meynet, G. 1997, A&A, 321, 452
Arnould, M., Goriely, S., & Meynet, G. 2006, A&A, 453, 653
Diehl, R. 2006, New Astron. Rev., 50, 534
Gounelle, M., Shu, F. H., Shang, H., et al. 2006, ApJ, 640, 1163
Grevesse, N., Noels, A., & Sauval, A. J. 1996, ASPC, 99, 117
Iliadis, C., D'Auria, J. M., Starrfield, S., & Wiescher, M. 2001, ApJS, 134, 151
Karakas, A., & Lattanzio, J. C. 2007, PASA, 24, 103
Knödlseder, J. 2008, Thèse d'Habilitation à Diriger des Recherches (HDR), Université Paul Sabatier, Toulouse (unpublished)
Knödlseder, J., Weidenspointner G., Jean, P., et al. 2008, in press [arXiv:0712.1668]
José, J., Hernanz M., & Coc, A. 1997, ApJ, 479, L55
Limongi, M. & Chieffi, A. 2006, ApJ, 647, 483
Meyer, B. S., & Zinner, E. 2006, in Meteorites and the Early Solar System II, ed. D. S. Lauretta, & H. Y. McSween Jr. (Tucson: Univ. of Arizona Press), 69
Mowlavi, N., & Meynet, G. 2000, A&A, 361, 959
Mitler, H. E. 1977, ApJ, 212, 513
Ouellette, N., Desch, S. J., & Hester, J. J. 2007, ApJ, 662, 1268
Palacios, A., Meynet, G., Vuissoz, C., et al. 2005, A&A, 429, 613
Prantzos, N., & Aubert O. 1995, A&A, 302, 69
Prantzos, N., & Diehl, R. 1996, Phys. Rep., 267, 1
Reimers, D. 1975, Problems in stellar atmospheres and Envelopes, ed. B. Baschek, W. H. Kegel, & G. Traving (Berlin Heidelberg New York: Springer-Verlag)
Sackmann, I.-J., & Boothroyd, A. I. 1991, ApJ, 366, 529
Siess, L. 2006, A&A, 448, 717
Siess, L. 2007a, A&A, 476, 893, Paper I
Siess, L. 2007b, ASP Conf. Ser. 378, 9
van Raai, M. A., Lugaro, M., Karakas, A. J., & Iliadis, C. 2008, A&A, 478, 521
Vassiliadis, E., & Wood, P. R. 1993, ApJ, 413, 641
Ventura, P., & D'Antona, F. 2005, A&A, 431, 279
Wadhwa, M., Amelin, Y., Davis, A. M., et al. 2007, in Protostars and Planets V, ed. B. Reipurth, D. Jewitt, & K. Keil (Tucson: Univ. of Arizona Press), 835